Article:
Maavara, T orcid.org/0000-0001-6677-9262, Brinkerhoff, C, Hosen, J et al. (5 more authors) (2023) Watershed DOC uptake occurs mostly in lakes in the summer and in rivers in the winter. Limnology and Oceanography, 68 (3). pp. 735-751. ISSN 0024-3590

https://doi.org/10.1002/lno.12306

Watershed DOC uptake occurs mostly in lakes in the summer and in rivers in the winter

Taylor Maavara[1,2*], Craig Brinkerhoff[3], Jacob Hosen[4], Kelly Aho[1,5], Laura Logozzo[1], James Saiers[1], Aron Stubbins[6], Peter Raymond[1,2]

[1] School of the Environment, Yale University, New Haven, CT, USA
[2] Yale Institute for Biospheric Studies, Yale University, New Haven, CT, USA
[3] Department of Civil and Environmental Engineering, University of Massachusetts, Amherst, MA, USA
[4] Department of Forestry and Natural Resources, Purdue University, West Lafayette, IN, USA
[5] National Ecological Observatory Network, Boulder, CO, USA
[6] Department of Marine and Environmental Sciences, Civil and Environmental Engineering, and Chemistry and Chemical Biology, Northeastern University, Boston, MA, USA

*Correspondence to: t.maavara@leeds.ac.uk. Current address: School of Geography, Faculty of the Environment, University of Leeds, Leeds, UK

Running head: A new model for river-lake DOC cycling

Keywords
dissolved organic carbon, inland waters, photomineralization, respiration, terrestrial DOC loading, gross primary productivity, watershed modeling

Key points

- Total riverine DOC uptake does not vary with stream order, but the proportion from photomineralization vs. biomineralization changes with stream order, flow, and temperature.
- Photomineralization is the dominant riverine form of mineralization.
- Lake biomineralization accounts for 80% of summer DOC uptake across an entire watershed, while river photomineralization accounts for at least half of winter DOC uptake.

Abstract

River networks transport dissolved organic carbon (DOC) from terrestrial uplands to the coastal ocean. The extent to which a reach or lake within a river network uptakes DOC depends on the stream order, the seasonal conditions, and the flow. At the watershed scale, it remains unclear whether DOC uptake is dominated by biological processes such as respiration, or abiotic processes like photomineralization. The partitioning of DOC uptake in lakes versus rivers is also unclear. In this study, we present a new model that unifies year-round controls on DOC cycling for an entire river network, including river-lake connectivity, to elucidate the importance of biotic vs. abiotic controls on DOC uptake. We present the **C**atchment **Up**take and **S**inks by Season, **O**rder, and **F**low for **DOC** (CUPS-OF-DOC) model, which quantifies terrestrial DOC loading, gross primary productivity (GPP), and uptake via microbes and photomineralization. The model is applied to the Connecticut River Watershed, and accounts for cascading reach- and lake-scale DOC cycling across ninety-eight scenarios spanning combinations of flows, seasons, and stream orders. We show that riverine DOC uptake is nearly constant with stream order, but the proportion of DOC uptake from photomineralization varies. Photomineralization dominates in rivers in most flow conditions and stream orders, especially in winter, accounting for at least half of whole-watershed DOC uptake in February across all flows. Whole-watershed summer DOC uptake occurs mostly via biomineralization in lakes, accounting for 80% of DOC uptake during the growing season, despite accounting for less than 6% of watershed open water surface area.

1. Introduction

River drainage networks are an integral component of the Earth's biogeochemical engine. Theory around drainage networks is often traced to the River Continuum Concept (Vannote et al., 1980), which describes river networks as a continuously changing series of physical and hydrological gradients from headwaters to downstream, which drive the associated continuum of biological processes, communities, and constituents. Dissolved organic matter (DOM), which plays a critical role in river network metabolism and is an important source of carbon to the oceans (Raymond and Spencer, 2015; Schlesinger and Melack, 1981), has been described as "watershed tea" due to the complexity and diversity of organic compounds that it integrates from sources throughout a watershed (Creed et al., 2015; Kaplan and Cory, 2016; Tank et al., 2010). The River Continuum Concept uses Strahler stream order, i.e., the classification system that is based on the number of tributaries upstream, to characterize general trends in longitudinal ecosystem metabolism with regard to the ratio between gross primary production (GPP) and ecosystem respiration (ER). DOM, which is approximately half dissolved organic carbon (DOC) by mass, varies in composition in response to differences in DOM sources (terrestrial loading vs. GPP) and in-stream uptake.

Cole et al. (2007) expanded on concepts of carbon loss from the aquatic continuum, including DOM uptake outlined in the River Continuum Concept, by formalizing the importance of inland water systems as active conduits or "leaky pipes" in carbon cycling from headwaters to oceans. Lakes, reservoirs, wetlands, floodplains, and rivers themselves can act as reactors, facilitating biogeochemical transformation processes that result in physical or biological DOC loss from the water column via microbial uptake including respiration, photodegradation, flocculation processes, and gaseous emissions, or addition via atmospheric fixation (photosynthesis) (Battin et

al., 2009; Raymond et al., 2013; Regnier et al., 2013). This DOC uptake has important implications for the global carbon cycle in that it controls the amount of carbon that is transferred laterally from the continents to the oceans, as well as the extent of vertical carbon dioxide fluxes from inland waters that can arise when DOC is mineralized to inorganic carbon (Raymond et al., 2013).

Numerous studies have built on Cole et al. (2007)'s leaky pipe conceptualization and used the River Continuum Concept's backbone connecting biogeochemical processes to stream order to elaborate on the controls of DOC uptake along the aquatic continuum (Abril and Borges, 2019; Battin et al., 2009; Bertuzzo et al., 2017; Fasching et al., 2016). Raymond et al. (2016) proposed the Pulse-Shunt Concept, which postulates that there are flows above which DOC fluxes moving downstream are high and uptake is low, creating transport-dominated DOC "shunts". Below these flows, river systems are reaction-dominated and DOC uptake is high. Wollheim et al. (2018) proposed the River Network Saturation concept, which states that a river's capacity to eliminate, transform, or retain a constituent decreases as flow increases. They postulate that as flow increases, both river supply and demand for a constituent also increase, with supply increasing more quickly, leading to river saturation and "shunting" of the constituent downstream. In both these conceptual models, the amount of DOC uptake is dependent on river network characteristics and the DOC reactivity. Despite these convergent model conceptualizations, it remains unclear how relative DOC uptake varies by stream order as flows and seasons change.

The Pulse-Shunt Concept and River Network Saturation dealt with in-stream reactions by considering a lumped DOC uptake flux but did not quantify how individual reactions such as respiration and photomineralization vary with flows, stream order, and season. These processes

have been quantified individually for several watersheds (Casas-Ruiz et al., 2017; Mineau et al., 2016; Wollheim et al., 2015). A recent study by Maavara et al. (2021) showed that across flows, photomineralization is a negligible sink relative to lateral DOC fluxes in a large temperate river network, but it remains unclear how important photomineralization is in lakes and relative to biomineralization (i.e., microbial uptake including respiration). In two studies conducted in the same Arctic rivers, results from one study showed that photomineralization accounts for a majority of total in-stream mineralization (Cory et al., 2014), while another showed that biomineralization dominates (Rocher-Ros et al., 2020). Without explicitly accounting for differences in flow, stream order, and season, it is difficult to reconcile contradictions in the literature. Furthermore, despite the interconnected nature of drainage networks, researchers have mainly quantified large-scale watershed DOC measurements in either rivers (Bertuzzo et al., 2017; Harrison et al., 2005; Zarnetske et al., 2018) or waterbody datasets composed of thousands of lakes and/or reservoirs (Maavara et al., 2017; Sobek et al., 2007), without explicitly accounting for whole-watershed connectivity of both types of systems. There is ample evidence that connected lakes fundamentally regulate downstream carbon transport through river networks (Brinkerhoff et al., 2021; Futter et al., 2008; Gardner et al., 2019).

A comprehensive watershed DOC model that incorporates the cascading reach- and lake-scale DOC sources, sinks, and fluxes across variable flows and seasons does not exist. As a result, quantifying the dependence of DOC uptake mechanisms on changing flows and temperatures at all stream orders, and subsequently linking DOC cycling quantitatively to the River Continuum Concept, has not been possible. However, using available high-resolution hydrological data products (Buto and Anderson, 2020), as well as drawing from advances in machine learning

119 algorithms used to predict riverine metabolism (Segatto et al., 2021), it is now possible to construct
120 such a model at the scale and resolution needed to address this short-coming. Therefore, in this
121 study, we advance the application of the River Continuum Concept to DOC uptake in watersheds.
122 Our study's aims are to quantify the relative importance of biotic vs. abiotic DOC uptake processes
123 (biomineralization and photomineralization) across stream orders, as well as quantify the seasonal
124 and flow conditions in which photomineralization or biomineralization may or may not dominate
125 total DOC uptake across stream orders. We apply these goals both to rivers and lakes to address
126 the relative importance of lentic vs. lotic systems in terms of whole-watershed DOC uptake.
127
128 We develop a spatially explicit mass balance model of DOC sources, sinks, and transport through
129 the Connecticut River watershed in the northeastern United States and southern Canada. An
130 existing body of literature dedicated to quantifying Connecticut River watershed metabolism,
131 carbon dynamics, and hydrology make the Connecticut an ideal watershed for such an exercise, as
132 ample information is available to parameterize a model (Aho et al., 2021a; Aho et al., 2021b;
133 Brinkerhoff et al., 2021; Hosen et al., 2019; Hosen et al., 2021; Maavara et al., 2021; Yoon et al.,
134 2021). We track terrestrial DOC loading, production via gross primary productivity (GPP),
135 consumption by microbial uptake (biomineralization) and photomineralization and the cascading
136 downstream transport through 98,254 stream reaches and lake segments at an average length
137 resolution of 511m, from first order through 8^{th}-order streams, rivers, ponds, lakes, and reservoirs.
138 Our model, which incorporates sources and uptake of DOC, which is sometimes called watershed
139 tea (Kaplan and Cory, 2016), is named "**C**atchment **Up**take and **S**inks by Season, **O**rder, and **F**low
140 for **DOC**", i.e., CUPS-OF-DOC. Rather than modeling a specific period in watershed history, we
141 calculate flows and water residence times at a suite of seven annual flow exceedance probabilities

specific to each stream reach and lake segment and apply them to twelve months of the year. This approach allows us to evaluate the full suite of transport conditions possible in all seasons and quantify flow-dependencies on DOC sources and sinks across stream orders at reach and/or lake scale.

2. Methods

All acronyms and model parameters provided in this section are defined both in the text and summarized in Table S1.

2.1 Field data collection and laboratory analyses

The Connecticut River watershed is a temperate 8th-order 29,200-km^2 basin flowing from Québec, Canada, through Vermont, New Hampshire, Massachusetts, and Connecticut, emptying to the Long Island Sound, a tidal estuary of the Atlantic Ocean. It is the largest watershed in the New England region of the United States, providing 70% of the freshwater entering Long Island Sound. It is 79% forested, about 5% urbanized, 4% wetland, and 8.5-12% agricultural (Clay et al., 2006).

Data collection was conducted from 2015 to 2017 in two sub-watersheds: the Farmington River watershed in northwestern Connecticut, and the Passumpsic River watershed in northeastern Vermont (Table 1, Fig. 1). Additional data was collected on the 8th-order Connecticut River mainstem in Thompsonville, Connecticut. Samples were analyzed for DOC concentrations and UV-Vis absorbance at 1-nm intervals from 200-800nm. Full method details are available in Hosen et al. (2021). Sites were located at existing United States Geological Survey monitoring locations where discharge (Q) data is reported online (USGS, 2020), except Jack Brook, Vermont. Field

165 DOC concentration datasets were supplemented with USGS monitoring at the same sites plus two

166 sites in Massachusetts and New York (details in section 2.3.1).

167

Table 1: Measurement sites used to calibrate terrestrial DOC loads or to evaluate model output (THOM), including US Geological Survey (USGS) site number, mean DOC concentration from the measurements gathered, timeframe of data collection, total upstream watershed area, stream area, and percent of upstream watershed that is classified as wetland according to the National Land Cover Database (NLCD 2016). Jack Brook, VT does not have a USGS site number and is located at 44.6946°N, 71.8468°W.

Site abbreviation	Site name, state	USGS site no.	n	Mean DOC (mg/L)	Timeframe	A_T (km^2)	Stream order	% upstream wetland
W9	W9, VT	01135100	3203	2.0	1991-2016	0.4	1	0
JACK	Jack Brook, VT	NA	421	2.9	2015-2016	2.85	1	0
POPE	Pope Brook, VT	01135150	158	3.0	2008-2017	10.0	3	1
BUNN	Bunnell Brook, CT	01188000	139	3.4	2015-2017	10.3	3	10
NEVE	Neversink River, NY	01435000	1308	2.2	1991-2019	66.6	5	0.6
GREE	Green River, MA	01170100	89	1.5	2012-2019	106.6	4	1.8
SLPR	Sleeper's River, VT	01135300	146	3.4	2008-2017	110.5	4	2
STIL	Still River, CT	01186500	154	5.1	2015-2017	221	5	7
PASS	Passumpsic River, VT	01135500	86	5.3	2015-2017	1124	6	4
FARM	Farmington River, CT	01189995	198	3.9	2015-2017	1492	6	7
THOM	Thompsonville, CT	01184000	144	3.5	2012-2019	25001	8	5

168

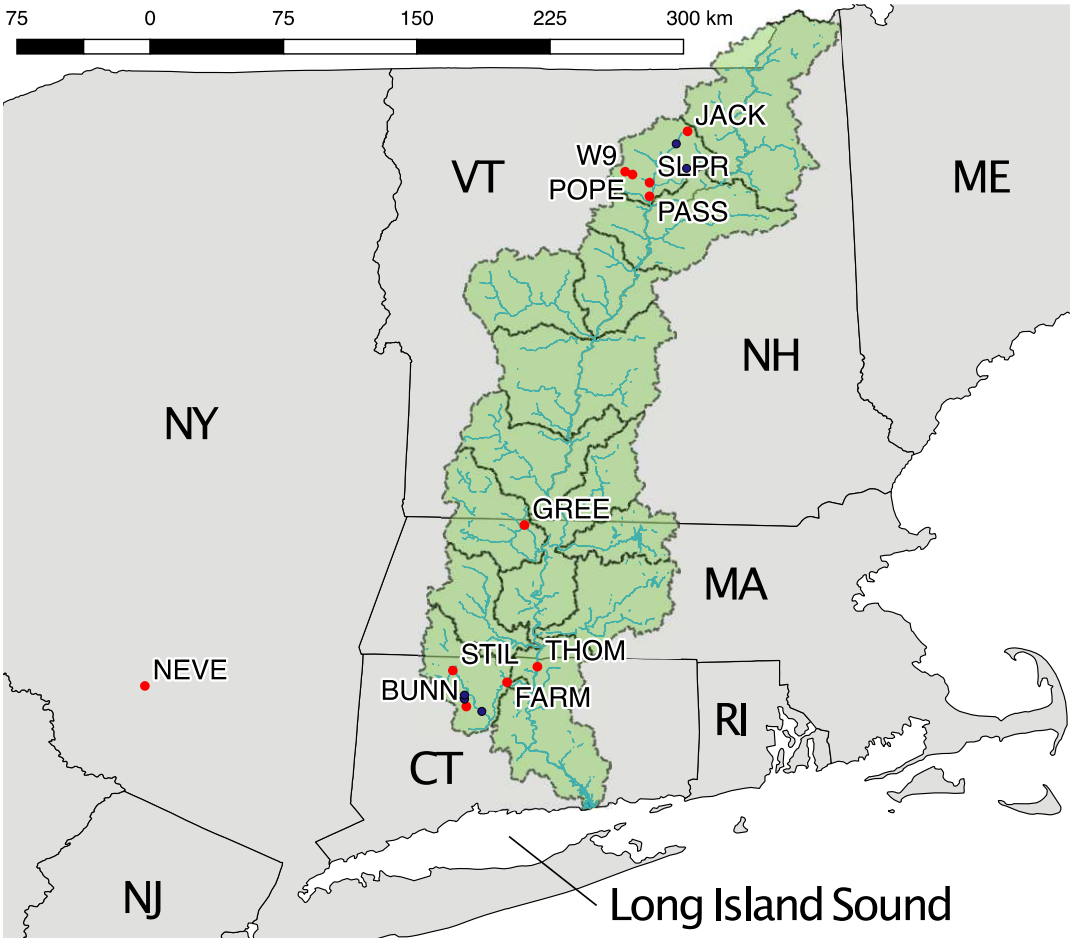

Figure 1: Map of the Connecticut River Watershed in green, with 6th-order sub-watershed boundaries outlined in black and the river network in blue. Red dots show the data collection (section 2.3.1) sites. Site information is available in Table 1. Navy blue dots show locations of five additional sites within the Farmington and Passumpsic River sub-basins for which GPP estimates were calculated in Hosen et al. (2019) and used to calibrate the riverine GPP fluxes in this model (section 2.3.2).

2.2 Hydrographic framework

The watershed is discretized into 98,254 river reaches and lake, reservoir or pond segments according to the NHDPlus HR dataset (Buto and Anderson, 2020; Moore et al., 2019). Throughout, we will refer to all lentic systems (which includes lakes, ponds and about 980

reservoirs connected to the river network) as "lakes." While NHDPlus HR provides the names for 11% of the lentic water bodies, which include ponds, lakes, and reservoirs, different types of lentic systems are not separated and so we do not classify them individually, nor are we able to identify what types of ponds are included. In general, NHDPlus HR reaches are discretized based on a network topology (when new tributaries join or a waterbody intersects the river). As a result, rivers of all stream orders are broken into multiple reaches, including first-order tributaries (which are frequently segmented by ponds). Large lakes are broken into multiple lake segments if there are multiple river inputs and/or outputs to the lake. Watershed lake and river surface areas, combined lengths, and percent of reaches that are dry for the range of flow scenarios are given in Table S2. For each reach and lake segment, we calculate both reach-specific hydraulic residence time (HRT_i, seconds) and cumulative hydraulic residence time ($HRT_{c,i}$, seconds), needed to model the change in DOC lability (Section 2.3.3), according to:

$$HRT_i = \begin{cases} \frac{L_i}{V_i}, & if\ river \\ \frac{Vol_i}{Q_i}, & if lake \end{cases} \quad (1)$$

$$HRT_{c,i} = \frac{\sum_2^{nu}(HRT_{c,i}Q_i)}{\sum_2^{nu}(Q_i)}, + HRT_i \quad (2)$$

$HRT_{c,i}$ reflects the average travel time of an individual parcel of water through the drainage network through surface water and shallow hyporheic zones, i.e. from the average headwater reach to each reach i. To calculate $HRT_{c,i}$ for each reach i, we took the reach-defined HRT_i (Eq. 1, where L_i is reach length (meters), V_i is mean flow velocity for each reach (m s^{-1}), obtained using the approach in Dingman (2007), i.e., imposing the hydraulic geometry of a rectangular river channel on Manning's equation, Vol_i is waterbody volume (m^3), and Q is streamflow, m^3 s^{-1}) and sequentially aggregated these values as we moved downstream in the network through both rivers

and lakes (Eq. 2, where *i* is the reach at hand and *nu* is the number of reaches directly upstream of reach *i*). This approach has been previously applied to the Connecticut River watershed in Brinkerhoff et al. (2021), where full method details related to these calculations are available. In cases where multiple reaches flow into one reach, the $HRT_{c,i}$ directly upstream of the current reach is calculated as the average $HRT_{c,i}$ for the upstream reaches and weighted by discharge to favor larger rivers (Eq. 2). After calculating HRT_i for every reach in the network, we estimate $HRT_{c,i}$ by running Eq. 2 sequentially, from the headwaters to the outlet.

We constructed flow duration curves for each reach via streamflow routing as well as explicit modeling of volumes for all 14,563 lakes. Following Brinkerhoff et al. (2021), we built flow duration curves for each reach by routing daily discharge through the river network and constructing flow-duration curves from those daily records. Daily discharge was itself constructed from Lin et al. (2019)'s daily runoff forcings for 1979-1989 (as a case study) and routed via the Hillslope River Routing model (Beighley et al., 2009). Ultimately, we estimated $HRT_{c,i}$ for Brinkerhoff et al. (2021)'s seven different 'characteristic annual discharges' at all 98,254 reaches. These 'characteristic annual discharges' are named Q_2, Q_{10}, Q_{25}, Q_{50}, Q_{75}, Q_{90}, Q_{98} and refer to the mean daily streamflows for each reach that are exceeded that percent of the time over the course of a year, and were calibrated using 10 years of measured flow data (Brinkerhoff et al., 2021). Finally, at low flows (e.g., Q_{98}, Q_{90}) many first-order streams have a flow of 0 m^3/s (Table S2). We define these as 'dry' reaches and they were ignored in the $HRT_{c,i}$ calculations by starting the $HRT_{c,i}$ calculations downstream of the dry segments.

Discharge-dependent reach segment widths, W_i in meters, are calculated using the empirical relationship from Raymond et al. (2013) from 9811 USGS stream gauging stations:

$$\ln(W_i) = 0.51 \ln Q_i + 1.86 \quad (3)$$

where Q_i is in $m^3\ s^{-1}$. The model is solved for steady-state conditions assuming a uniform characteristic flow condition (see Section 2.4) across the entire network. Because the model is run under a characteristic flow frequency, downstream hydraulic geometry is used to initialize reach segment widths, W_i in meters (Eq. 3), that correspond to that flow frequency (Brinkerhoff et al., 2019; Gleason, 2015; Leopold and Maddock, 1953; Moody and Troutman, 2002). These are independent of at-a-station variability and reflect the downstream variation in river width for our flow frequency. Water column depth, $z_{wc,i}$, is calculated first by obtaining the water volumes (Vol_i in m^3) by multiplying the above-derived HRT_i (day) by Q_i ($m^3\ day^{-1}$), and computing $z_{wc,i}$ as the missing dimension using Vol_i, L_i and W_i. A breakdown of the hydrological continuity equations is given in Section S1. All time units are then converted into days for use in the DOC model (Section 2.3).

2.3 DOC model

We represent DOC mass in each of the 98,254 river reaches and lake segments as discretized by the NHDPlus HR. The ordinary differential mass balance equation representing DOC for each reach or water body segment, i, is

$$\frac{dDOC_i}{dt} = ter_i + GPP_{DOC,i} - k_{r,i} DOC_i - k_{\psi,i}\, DOC_i + \sum_2^{nu} DOC_i - \frac{1}{HRT_i} DOC_i \quad (4)$$

The model solves for the total DOC mass in mg-C in the full water column in each NHDPlus HR reach i at each timestep t. ter_i is the terrestrial DOC load (mg-C day^{-1}) to each reach i from the directly adjacent local subwatershed zone, A_i, calculated using a regression approach with discharge and upstream wetland area as explanatory variables (see Section 2.3.1 for regression development). A_i differs from the total upstream watershed area, A_t, as it only includes individual catchment (that is, it is capturing any water added directly to each reach, not including upstream water), rather than the total upstream contributing area. $GPP_{DOC,i}$ is gross primary productivity (mg-C day^{-1}) in each lake segment or river reach i (Section 2.3.2). k_r is the first-order kinetic rate constant (day^{-1}) describing the biological mineralization of DOC (Section 2.3.3). $k_{\psi,i}$ is the first-order rate constant for complete photooxidation (i.e., photomineralization) of DOC to CO_2 (mg-C day^{-1}) in reach i (modeled according to methods described in Section 2.3.4). $\sum_2^{nu} DOC_i$ describes the sum of DOC from reaches or tributaries directly upstream of reach i, *nu,* if applicable. The final term represents the flux exiting the reach going downstream, which is a function of the flushing rate (day^{-1}) equivalent to the inverse of the water residence time (1/*HRT*). Dependence of the efflux term on *HRT* controls the magnitude of the in-stream processes; the longer the *HRT*, the larger the magnitude of in-stream fluxes (e.g., according to the mathematical formulation initially presented for phosphorus loss in lakes by Vollenweider (1975)) leading to smaller effluxes downstream. To obtain DOC concentrations, [*DOC*], from the DOC_i masses output by the model, the DOC_i masses are divided by Vol_i.

2.3.1 Terrestrial DOC loading

In this section we present a streamlined explanation of how terrestrial DOC loading was modeled. A step-by-step breakdown is available in the Supplementary Material, Section S2. We augmented our datasets of streamwater flows and DOC concentration with data from the USGS National Water Quality Information Systems at 11 sites within or near the Connecticut River watershed (Section 2.1) (Table 1). We searched existing and historical USGS monitoring sites within the New England region, including eastern New York. Sites with fewer than 85 DOC measurements or with temporal gaps exceeding two months were not included because the data were insufficient to estimate parameters governing the relationship between DOC concentration and discharge. The Weighted Regression by Time, Discharge, and Season (WRTDS) model (Hirsch et al., 2010) was applied to sites on 6th-order rivers or lower to estimate monthly concentration-discharge relationships of the form

$$[DOC] = aq^b \quad (5)$$

where $[DOC]$ is in mg-C L^{-1}, q is the specific discharge (Q divided by total upstream watershed area A_t) in m^3 s^{-1} watershed km^{-2}, and a and b are unitless coefficients for each monthly equation at each site (Table S3). DOC concentrations in rivers above 6th-order tend to be controlled to a larger extent by in-stream processes rather than terrestrial loading, and thus show more chemostatic properties (i.e. the slope b in Eq. 5 is approximately 0), not reflective of the terrestrial loading trends we are constraining in this portion of the model (Creed et al., 2015; Hosen et al., 2021). All sites in Table 1 except Thompsonville fall into this criterion, leaving 10 calibration sites. Thompsonville data was used to compare model trends with measurements (Supplemental Material, Section S9).

We binned q values used in Eq. 5 into 10 intervals capturing the discharge distributions across three orders of magnitude of each of the calibration sites (Fig. S1). DOC concentrations at the center of each bin were computed using Eq. 5 for each month, and regressed against the fraction of wetland cover in the upstream watershed, p_w (unitless) for each site:

$$[DOC] = mp_w + u \quad (6)$$

where m and u are constants for each month and q bin (Table S4).

To scale this approach to each of the 98,254 reaches in the watershed, p_w was calculated for each of the adjacent local subwatershed A_i given in the NHDPlus HR database by spatially overlaying A_i with the National Land Cover Database (NLCD 2016) classification raster (woody wetlands + emergent herbaceous wetlands). DOC concentration for each reach was then computed using the monthly and flow-specific constants calibrated for Eq. 6 (Table S4), and converted to the terrestrial load term input into Eq. 4, ter_i, in mg-C day^{-1} by multiplying by Q. We assume that all Q in headwater streams is terrestrial in origin (but that DOC can also be generated via GPP, see Section 2.3.2), and for all other stream reaches and lake segments downstream, we calculate the difference in Q between reach i and reach $i+1$ and use this difference as the terrestrial Q.

2.3.2 Photosynthesis

To model GPP in rivers, we utilize previously published daily GPP rates from May 2015 – December 2017 generated by Hosen et al. (2019) from 15-min interval dissolved oxygen (DO) measurements using the R package *StreamMetabolizer* (Appling et al., 2018) for the Fig. 1 sites

in the Farmington and Passumpsic River watersheds. To capture seasonal variability, we trained separate random forest models for each month of the year on a total of 6621 GPP estimates from Hosen et al. (2019), ranging from 227-787 estimates for each month (see Section S3 for details and Table S8 for monthly random forest model performance statistics). Predicted GPP estimates were in g-O_2 m^{-2} day^{-1}. Each of the trained monthly random forest models were then applied to predict GPP in each segment of the watershed. To estimate the extracellular release of DOC from GPP, we calculated approximate C production from GPP in g-C m^{-2} day^{-1} using molar O_2:C ratios of 1-1.8 (Demars, 2019; Howarth and Michaels, 2000), applied to the relationships in Baines and Pace (1991), which provides an estimate of extracellular DOC release, to generate the following equation:

$$\ln\left(GPP_{DOC,i}\right) = -0.52 + 0.66\ln\left(GPP_{O2,i}\right) \quad (7)$$

where $GPP_{O2,i}$ is the GPP estimate in g-O_2 m^{-2} day^{-1} and $GPP_{DOC,i}$ is the DOC released via extracellular release of GPP-produced biomass, which is input into Eq. 4.

In lakes, GPP (mg-C day^{-1}) is calculated by extracting a reduced order model of photosynthesis from a modified version of the organic carbon Monte Carlo model developed for lakes by Lewis Jr (2011) and modified for reservoirs in Maavara et al. (2017). The model is based on the depth-integrated model (Behrenfeld and Falkowski, 1997; Reynolds, 2006; Vollenweider, 1970) that calculates GPP by estimating the chlorophyll-specific carbon fixation rate and depth-integrated chlorophyll concentration in the water body, from parameters including extinction coefficients for water, DOC, and suspended sediment, which block light, day length, mixing depth, temperature,

and latitude-specific monthly incoming solar irradiation. The full details of this approach are found in the Supplementary Information, Section S3, including Eq. S11-S14. To limit computational demands, we use these equations to produce a reduced order model. We run a Monte Carlo analysis of Eq. S11–S14 using distributions of lake temperature, surface area, depth, and DOC concentrations that were defined in Maavara et al. (2017). From this output, we generate a simplified equation for GPP at 25°C in water body i ($GPP_{25,DOC,i}$) that is used in the model:

$$GPP_{25,DOC,i} = 0.5381\ DOC_i^{0.8875};\ R^2 = 0.65 \quad (8)$$

$GPP_{DOC,i}$ for the given water temperature in each lake is then calculated using a $Q_{10} = 2.23$ (Coles and Jones, 2000). If the average monthly water temperature is less than 0°C, GPP is assumed to be zero for that water body.

2.3.3 Biomineralization

The DOC biomineralization (i.e., microbial uptake, including respiration) rate is modeled with a first-order kinetics reaction governed by the coefficient k_r (day^{-1}) in Eq. 4. We calculate k_r using the relationship derived by Catalán et al. (2016) that accounts for OC ageing, and subsequent decreased lability, as DOC moves from upstream to downstream. We use the cumulative water residence time ($HRT_{c,i}$) for each reach as a proxy for age, which accounts for all headwater and lateral water sources, and use only the freshwater rate constants calculated for bio-mineralization directly (i.e., excluding the field-measured rate constants that include impacts of GPP or photomineralization, which we model separately here) in Catalán et al. (2016):

$$k_{r,25,i} = 0.007\ HRT_{c,i}{}^{-0.611} \quad (9)$$

where $k_{r,25,i}$ is the rate coefficient at 25°C, which is corrected to reach-specific temperature using a temperature coefficient (Q_{10}) = 2 (Reynolds, 2006). If water temperatures are below 0°C, we assume bio-mineralization does not occur.

2.3.4 Photomineralization

Complete photooxidation of DOC to dissolved inorganic carbon (DIC) (i.e., photomineralization, ψ), in each river reach and lake segment is based on the formulation (Cory and Kling, 2018; Koehler et al., 2012; Maavara et al., 2021):

$$\psi = \int_0^{z_{wc}} \left(\int_{\lambda_{min}}^{\lambda_{max}} E_{0,\lambda} a_\lambda e^{-(K_{d,\lambda} z)} \phi_\lambda d\lambda \right) dz \quad (10)$$

where λ_{min} and λ_{max} are the maximum and minimum wavelengths (280-600nm), $E_{0,\lambda}$ is the daily downwelling irradiation (mol photons m^{-2} day^{-1} nm^{-1}), including the impacts of canopy cover shading, a_λ is the colored DOM absorption coefficient (m^{-1}), $K_{d,\lambda}$ is the vertical attenuation coefficient for downwelling irradiance in the water body (m^{-1}), z is the depth (m), and ϕ_λ is the apparent quantum yield (AQY, mg-C (mol photons)$^{-1}$ nm^{-1}), which describes the photolability of the DOC in each river reach and lake segment by quantifying the complete photomineralization of DOC to DIC. Depth- and wavelength-integrated ψ is calculated in units of mg-C m^{-2} day^{-1} and converted to mg-C day^{-1} by multiplying by reach length and width. The parameters a_λ, $K_{d,\lambda}$, ϕ_λ were constrained empirically using DOC concentration and absorbance field measurements collected in the watershed (Section 2.1). $E_{0,\lambda}$ was modeled using the SMARTS model v. 2.9.8

(Gueymard, 1995; Gueymard, 2019), combined with a canopy cover correction that we developed using canopy photographs and a bagged tree regress model. For details regarding how each of these parameters are modeled and constrained and how Eq. 10 is integrated across wavelengths for all reaches in the watershed for each month, refer to section S4 in the Supplementary Material, or Maavara et al. (2021).

Eq. 10 was previously calibrated and solved for all riverine reaches in the watershed in Maavara et al. (2021), discretized monthly and for the same characteristic flows and stream network as described in Section 2.2. This process of integrating Eq. 10 analytically for all Connecticut River watershed reaches is very computationally demanding. Therefore, in order to simplify the output and reduce computational needs associated with calculating photomineralization alongside all the other DOC fluxes at 98,254 reaches and lake segments in all flows and months for the watershed, we derive empirical relationships predicting first order rate constants for photomineralization, $k_{\psi,\mathrm{i}}$, from the output of Maavara et al. (2021), and model ψ for each reach i with first order kinetics:

$$\psi_i = k_{\psi,\mathrm{i}}\, DOC_i \tag{11}$$

For each month, we aggregate predicted photomineralization fluxes for all flows, and fit k_{ψ} with rational equations of the form:

$$k_{\psi,\mathrm{i}} = \frac{p_1 z_{wc,,i} + p_2}{z_{wc,i}{}^2 + h_1 z_{wc,i} + h_2} \tag{12}$$

where p_1, p_2, h_1, and h_2 are constants specific to each month (Table S5), and $z_{wc,i}$ is the water column depth (m) in reach *i*. This simplification still allows for all the controls on photomineralization that appear in Eq. 10 to be included, as Eq. 11 is still a function of DOC, which controls a_λ and $K_{d,\lambda}$, and in turn, ϕ_λ, and constraining Eq. 12 with different coefficients for each month incorporates for the differences in light availability and canopy cover. This form of equation was tested against other linear and non-linear fits and yielded the lower statistically significant R^2 for each month.

2.4 Model solutions

Eq. 4 was solved numerically by the fourth order Runge-Kutta method with a time step of 0.002 days, and the model is run from initial conditions of zero for DOC_i for each characteristic discharge and month for 90 model days, until all reaches are at or very close to steady state (see Supplementary Material Section S5 for details). We solve the model for average monthly conditions using seven characteristic discharges (Q_2, Q_{10}, Q_{25}, Q_{50}, Q_{75}, Q_{90}, and Q_{98}), which refer to cumulative frequency of the streamflows for each reach that are equaled or exceeded that percent of the time (Searcy, 1959). For instance, Q_{50} represents median annual flows calculated specifically for each reach, while Q_2 and Q_{98} represent extreme flood (Q_2 or flows exceeded 2% of the time) and low-flow events (Q_{98} or flows exceed 98% of the time) of the observed annual record, respectively. Solving for each of the seven annual flow conditions, combined with temperature and climate conditions for each month enables us to quantify a matrix of 98 model scenarios combining the seven annual flow scenarios with climatic variables for the twelve months of the year to explore watershed behavior fully. Thus, while we might expect very high flow conditions to occur predominantly in the spring snowmelt period, for example, this approach

allows us to evaluate all combinations of transport and reaction conditions possible, even if they are unlikely.

Reach segments are routed by tracking the flow of water and DOC from upstream reach(es) based on the upstream reach indexed in NHDPlus HR. Our routing follows the major flow path through the watershed; in cases where the river diverges (e.g., canals, aqueducts), we route DOC through the main channel as defined in NHDPlus HR's Divergence index.

2.5 Relative DOC elimination calculation

Several indices have been used in the literature to quantify the relative magnitude of biogeochemical processes, including the uptake of DOC compared with total DOC flux through a water body (Marzadri et al., 2017; Stream Solute Workshop, 1990; Wollheim et al., 2018). One such example commonly used in rivers is the uptake velocity, v_f, which, when applied to DOC describes the first-order rate of DOC consumption relative to the water surface, allowing for variability with changing concentrations (Wollheim et al., 2018). For each reach or lake segment, we calculate v_f, in m day^{-1}, by dividing the surface area-normalized bio-mineralization flux plus photomineralization flux (mg-C m^{-2} day^{-1}) by the DOC concentration (in mg-C L^{-1}) multiplied by 1000 (to convert L to m^3) (Stream Solute Workshop, 1990; Wollheim et al., 2018) (Figure S6 and S8). Using v_f, we calculate a per-reach elimination, R_i (unitless), describing the relative change in DOC:

$$R_i = 1 - \exp\left(\frac{-v_{f,i}}{H_l,i}\right) \quad (13)$$

where $H_{l,i}$, the hydraulic load (m day^{-1}), is calculated according to:

$$H_{l,i} = \frac{Q_i}{L_i w_i} \quad (14)$$

where Q_i is in m^3 day^{-1} and reach length, L_i, and width, w_i, are in m (Mineau et al., 2016). R_i varies between 0 and 1, where 0 indicates none of the reach DOC is consumed, and a value of 1 indicates 100% of the DOC in the reach is consumed. Eq. 13 is an indicator of the relative importance of reaction rates, represented by $\upsilon_{f,i}$, to transport rates, represented by $H_{l,i}$. In reaction dominant systems, R_i is closer to 1, while in transport dominant systems, R_i is closer to 0. In lakes, R_i, is more conventionally calculated as:

$$R_i = \frac{DOC_{in} - DOC_{out}}{DOC_{in}} \quad (15)$$

where DOC_{in} and DOC_{out} are fluxes of DOC entering and exiting the lake. A negative R_i indicates a net addition of DOC to the water body via GPP.

The proportion of total mineralization that is from photomineralization, ρ_p, in each reach or lake segment *i* is calculated as

$$\rho_{p,i} = \frac{k_{\psi,i}\, DOC_i}{k_{r,i} DOC_i + k_{\psi,i}\, DOC_i} \quad (16)$$

3. Model Output and Discussion

In this section, we present the results of CUPS-OF-DOC and evaluate its performance in the context of existing literature. In line with the goals of this paper, we focus specifically on DOC uptake fluxes in the main text and present terrestrial loading and GPP results in the Supplementary Material, Sections S6-S8, Fig. S4. To streamline data presentation, we give results for the months of February and August, which best represent end-member winter and summer fluxes for each process in the model. We reiterate that our model output assumes that all stream reaches and lake segments are experiencing the same flow scenario (as calibrated for each specific reach) at the same time, and that each flow scenario is calculated for all model months, generating a matrix of possible flows with possible monthly conditions, even if they are unlikely in the watershed itself (e.g., Q_2 flows in August). This amounts to a continuum-of-scenarios analysis of flow, temperature sensitivity, and light availability on DOC across stream orders. As a result, a traditional validation against measured data does not yield meaningful insights into the model performance, as we do not attempt to reproduce a time series of measured data. We do however compare concentration-discharge trends with Thompsonville measurements in Section S9 to provide some assessment of model quality. Given that each flux in the model is calibrated using measurements from the watershed, our goal here is to show that model output is reasonable in the context of existing literature ranges, rather than trying to exactly reproduce time series of DOC concentrations at specific places and times.

3.1 Magnitudes of DOC uptake fluxes

Biomineralization fluxes average 3.7 x10^3 mg-C m^{-2} day^{-1} in lakes and 27.6 mg-C m^{-2} day^{-1} in rivers in August at Q_{50} flows (Fig. 2a). In February these means decrease to 88.6 mg-C m^{-2} day^{-1} in lakes and 1.4 mg-C m^{-2} day^{-1} in rivers at Q_{50}. In August, biomineralization increases at Q_2 to

163.8 mg-C m^{-2} day^{-1} in rivers and 9.3 x 10^3 mg-C m^{-2} day^{-1} in lakes, and decreases at Q_{98} to 6.5 mg-C m^{-2} day^{-1} in rivers and 2.9 x10^3 mg-C m^{-2} day^{-1} in lakes. Temperature broadly controls biomineralization across seasons, due to the dependence of $k_{r,i}$ on temperature, but there are not clear empirical trends between DOC uptake relative to water column DOC fluxes (Fig. S6). Biomineralization increases at higher flows for two main reasons: (1) more DOC is available due mainly to higher terrestrial loading (Fig. S4c, f, i), and (2) the newly loaded or produced DOC is fresh and labile due to shorter water residence times and therefore larger k_r (Eq. 9). Biomineralization in both rivers and lakes tends to be lower at higher stream orders because it has aged during its transport through the watershed. For example, in August, 8th-order streams average biomineralization rates of 25.5 mg-C m^{-2} day^{-1} at Q_{50} flows, compared with 38.9 mg-C m^{-2} day^{-1} in 1st-order streams. For the same river field measurement sites as in Fig. 1, Hosen et al. (2019) determined respiration fluxes averaging 3.7 x 10^3 mg-O_2 m^{-2} day^{-1} for May-October, with values ranging from 6.9 mg-O_2 m^{-2} day^{-1} to 51 x 10^3 mg-O_2 m^{-2} day^{-1}, which can approximately be converted to 2.6 mg-C m^{-2} day^{-1} to 20 x 10^3 mg-C m^{-2} day^{-1}, assuming a molar respiratory quotient of 1 to convert rates from grams of oxygen to grams of carbon (Berggren et al., 2012; Demars, 2019; Williams and del Giorgio, 2005).

At Q_{50} flows, median photomineralization fluxes are 119 mg-C m^{-2} day^{-1} in lakes and 10.1 mg-C m^{-2} day^{-1} in rivers (Fig. 2a) in August, and medians of 0 in both lakes and rivers in February due to widespread ice coverage and low light availability. Median August photomineralization fluxes in rivers are 2.5 mg-C m^{-2} day^{-1} at Q_{98} flows and 8.5 mg-C m^{-2} day^{-1} at Q_2 flows, while median lake fluxes are 68.3 mg-C m^{-2} day^{-1} at Q_{98} and 32.9 mg-C m^{-2} day^{-1} at Q_2. The magnitude of photomineralization fluxes generally increases with stream order due to lower canopy shading,

larger river surface areas, higher DOC availability and to some extent, added depth. There is a correlation between increasing photomineralization and depth until a point; if the photic depth has not yet been reached, photomineralization will increase with depth. If photic depth has been reached, added depth will not increase photomineralization because the bottom of the water body is in the dark. Photic depths depend on the DOC concentration; note that as DOC concentrations increase, photic depth decreases but the depth-integrated photomineralization fluxes increase, with more photomineralization taking place progressively closer to the surface. A full discussion of the depth and DOC controls on photomineralization in rivers by stream orders and flows is given in Maavara et al. (2021). Our model outputs are in good agreement with the magnitudes of photomineralization fluxes found in other freshwater systems. Allesson et al. (2020) found average summer rates of 8.4-21.4 mg-C m^{-2} day^{-1} in 77 high latitude Norwegian and Swedish lakes, while Koehler et al. (2014) determined fluxes of 15.4-41.9 mg-C m^{-2} day^{-1} in Swedish lakes. Cory et al. (2014)'s high-Arctic lake and river values of 35.8 – 296 mg-C m^{-2} day^{-1} overlap with the upper range of the fluxes found by our data (Fig. 2a), and may exceed ours due to lower canopy cover, longer daylight hours during the summer months, and more photo-labile DOM (i.e., higher apparent quantum yields), which in CUPS-OF-DOC are modeled with empirical relationships from absorbance and DOC concentration measurements (Sections 2.3.4 and S4).

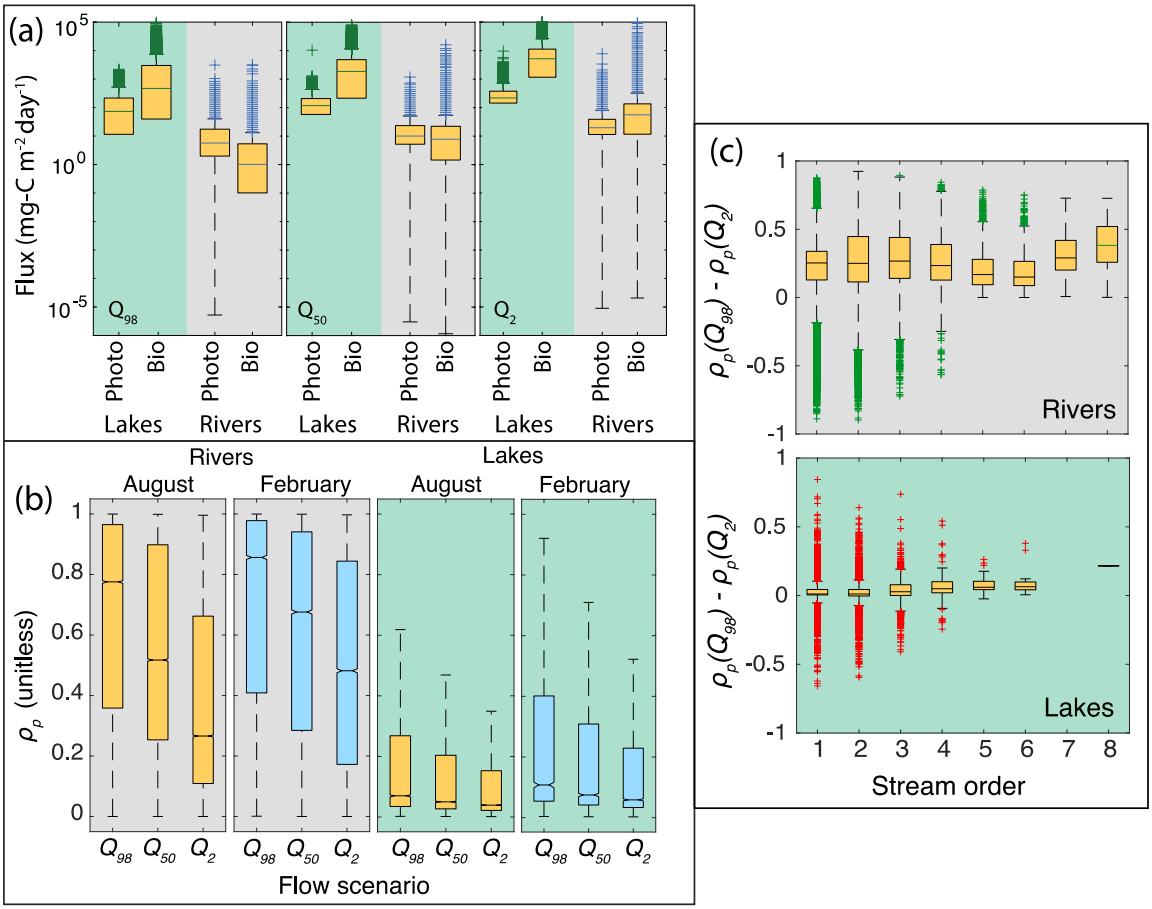

Figure 2: Panel (a): Model-generated magnitudes of fluxes for photomineralization and bio-mineralization in August in lakes and rivers for Q_2, Q_{50} and Q_{98} flows (mg-C m^{-2} day^{-1}), with center line representing median, edges are 1st and 3rd quartiles, and "+" symbols are outliers. Panel (b): Proportion of total mineralization (biomineralization plus photomineralization) that occurs via photomineralization (ρ_p, unitless) for lakes and rivers in August and February at Q_2, Q_{50} and Q_{98} flows. Note that outliers in lakes panels have been removed for clarity but extend from upper whiskers to 1.0. Middle line indicates median, box edges are 1st and 3rd quartiles. Panel (c): the change in ρ_p between Q_{98} and Q_2 flows for rivers and lakes in August by stream order. Positive values indicate ρ_p at Q_{98} flows are larger than at Q_2 flows.

3.2 Proportion of total mineralization

552 In rivers, we find that on average the proportion of total mineralization that occurs via
553 photomineralization, $\rho_{p,i}$, was 0.56 in August at median flows, with this value rising to 0.66 in Q_{98}
554 flows, and individual reaches varying from 0-1 across all flows throughout the watershed (Fig.
555 2b). In February, when water temperatures are low, an average of 0.70 and a median of 0.86 of the
556 total mineralization is from photomineralization at Q_{98} (Fig. 2b). For river reaches, flow variations
557 can alter ρ_p by $\pm$100%. In some reaches, mineralization occurs via biomineralization at Q_2 flows
558 and switches to mineralization mostly via photomineralization at Q_{98} flows, and vice versa, with
559 the range of possible variability highest at low stream orders (Fig. 2c). For example, at Q_{98} in a
560 small stream reach with little canopy cover and low DOC concentrations, photomineralization can
561 account for most of total mineralization because shallow depth allows essentially all DOC in the
562 water column to be exposed to solar irradiation. In such conditions, k_r can be comparatively small
563 if the reach is immediately downstream of, for example, a pond with a small trickle for an outlet,
564 creating a long water residence time, causing the DOC to age and lose lability. In the same reach
565 at Q_2, k_r can increase if the upstream pond residence time decreases in response to high flows and
566 the DOC remains fresh.
567
568 Our findings are similar to those of Cory et al. (2014), who found that $\rho_p = 0.70$-0.95 in Arctic
569 lakes and rivers, including both partial photooxidation (which we do not account for here) and
570 complete photooxidation. Our results additionally may help reconcile the differences in
571 conclusions between Cory et al. (2014) and Rocher-Ros et al. (2020). The latter compared the
572 photooxidation rates measured by Cory et al. (2014) from June-October 2011-2013 with two
573 weeks of metabolism measurements for the same Arctic rivers in July 2018 and found that
574 respiration fluxes were an order of magnitude larger than photooxidation fluxes, i.e., ρ_p was much

575 smaller than Cory et al. (2014) determined. Our highly flow-dependent results indicate that the
576 seemingly contradictory findings of Cory et al. (2014) (high ρ_p) and Rocher-Ros et al. (2020) (low
577 ρ_p) may be reconciled by temporal differences in flows and associated water residence times in
578 the sampling periods that do not overlap, where differences in ρ_p across flows can be especially
579 exaggerated at low DOC concentrations in small streams and rivers that have little or no canopy
580 cover. Discharge data from both studies would be needed to evaluate this hypothesis.
581
582 While the photomineralization areal fluxes in lakes are on average an order of magnitude larger
583 than in rivers, biomineralization fluxes in lakes are two orders of magnitude larger than in rivers,
584 corresponding to the same difference in orders of magnitude in residence time between rivers and
585 lakes (Fig. 2a, S3). Biomineralization can be much larger in lakes than rivers because it is not light-
586 limited and can occur below the photic zone. Conversely, photomineralization in lakes is limited
587 to the photic zone. Lakes are deeper than the photic zone more often than rivers, and so their
588 additional depth does not often allow for much higher fluxes than in rivers for a similar surface
589 area. As a result, ρ_p in lakes is much smaller than in rivers (Fig. 2b), averaging 0.18 (median =
590 0.05) in August at Q_{50} flows and rising only to 0.22 (median = 0.07) in February when
591 biomineralization is suppressed by cold temperatures. The difference in ρ_p across flow scenarios
592 is close to 0 in lakes on all stream orders, with low variability, and rising only slightly in lakes on
593 larger stream orders (Fig. 2c). This lack of change across flow scenarios is because changes in
594 flow, velocity, and volume do not alter the surface area of lakes as much as they do in rivers, and
595 thus the surface area (and near-surface DOC) available for sunlight to photooxidize remains
596 relatively constant.
597

598 **3.3 Relative water column DOC elimination**

599 Despite having shown that photomineralization can be important in river networks relative to
600 biomineralization, its importance is close to negligible relative to the magnitude of DOC fluxes in
601 both lakes and rivers. Maavara et al. (2021) considered the importance of photomineralization in
602 the Connecticut River watershed's river reaches in terms of its ability to eliminate DOC from the
603 water column and found that per-reach removal (R_i, Eq. 13) was 0.026-0.18% of the DOC flux at
604 median flows. They concluded that relative to the magnitude of DOC transport fluxes,
605 photomineralization is a negligible DOC consumption term in river reaches, as short residence
606 times do not allow sufficient time for much complete photochemical transformation to take place.
607 In this study, we build on the findings of Maavara et al. (2021) by now accounting for
608 biomineralization in rivers plus both mineralization processes in lakes. Our results show that the
609 total R_i for photomineralization and biomineralization combined in river reaches is on average
610 0.003 (i.e., 0.3%) at Q_{50} in August (Table 2). We calculate average lake segment eliminations (R_i,
611 Eq. 13 and 15) at Q_{50} flows of 0.039 (i.e., 3.9%) in August, with nearly 96% of this elimination
612 from biomineralization (Table 2).
613
614 The overall trend for lake segment R_i increases according to a power law relationship as residence
615 time increases, reaching more than 0.2 at residence times of 800-1000 days (Fig. S7). At median
616 flows, k_r in Connecticut River watershed lakes averages 0.013 day^{-1} in August and 0.0014 day^{-1}
617 in February, and is higher at high flows (Table 2). For similar k_r values, the R_i output by our model
618 for lakes is lower than the power relationship modeled in Hanson et al. (2011), where R_i was above
619 0.7 in lakes with residence times of about one year. However, it is difficult to directly compare our
620 results with theirs as they model lakes with residence times on the order of years, while we model

621 lakes with residence times on the order of 100 hours, with only a few lake segments exceeding 1
622 year residence time (Section S3, Fig. S3b). Our extended analysis shows here that while
623 photomineralization fluxes in lakes are one to two orders of magnitude larger than in rivers on
624 average, photomineralization is even less important relative to DOC transport fluxes through lakes,
625 with R_i values that never exceed 0.01 (1%) at residence times of 1000 days in any season (Fig. S7).
626
627 Across flows, riverine per-reach R_i is highest in low stream orders and decreases exponentially as
628 stream order increases (Fig. 3a, d, g). However, we see that this trend does not arise due to a
629 meaningful change in the magnitude of the total mineralization flux, which remains relatively
630 constant per unit surface area across stream orders (Fig. 3b, e, h). As discussed in Section 3.1,
631 biomineralization fluxes decrease with stream order due to the ageing of DOC and the associated
632 decrease in k_r, while photomineralization fluxes generally increase, driving relatively constant
633 total mineralization fluxes with stream order. The decrease in R_i therefore reflects the increase in
634 DOC flux moving through each reach as stream order increases rather than a decrease in the size
635 of the mineralization reaction flux. Note that the increase in total available DOC per stream reach
636 does not follow trends in DOC concentration (Fig. S3c-h); higher order reaches are wider and
637 deeper and thus can carry a larger total mass of DOC, which accumulates from upstream to
638 downstream as terrestrial and autochthonous DOC is added at a rate that exceeds mineralization
639 rates (Table 2). As flows increase, the magnitude of the total mineralization flux increases across
640 all stream orders (Fig. 3b, e, h), mostly reflecting the increase in biomineralization with flow
641 (Section 3.1).
642

643 The similar total mineralization fluxes across stream orders arises because of changing importance
644 of biomineralization compared with photomineralization (Fig. 3c, f, i). At Q_{98} flows, the proportion
645 of total mineralization from photomineralization, ρ_p, is lowest in first order streams (median =
646 0.22) and increases to 0.9 and above in 4th-order rivers and higher. At higher flows,
647 photomineralization becomes less important relative to biomineralization at all stream orders, due
648 to higher DOC concentrations and associated light extinction as well as a greater proportion of the
649 DOC occurring below the photic depth, with ρ_p peaking in 6th-order streams. The maximized ρ_p
650 in 6th-order rivers reflects the interplay between areal biomineralization fluxes, which generally
651 decrease as stream orders increase due to DOC ageing, especially at low flows, and areal
652 photomineralization fluxes, which generally increase up to 6th order before plateauing (with
653 exceptions at low stream orders in high flows, see Maavara et al. (2021) for details). Below 6th-
654 order, biomineralization of fresh DOC dominates while photomineralization is limited by
655 shallower stream depths, higher canopy cover, and low DOC availability. As flows increase in 6th-
656 order rivers and above, ρ_p decreases because enhanced mobilization of fresh terrestrial material
657 increases the overall freshness of DOC, driving higher biomineralization fluxes per unit area (Fig.
658 3).

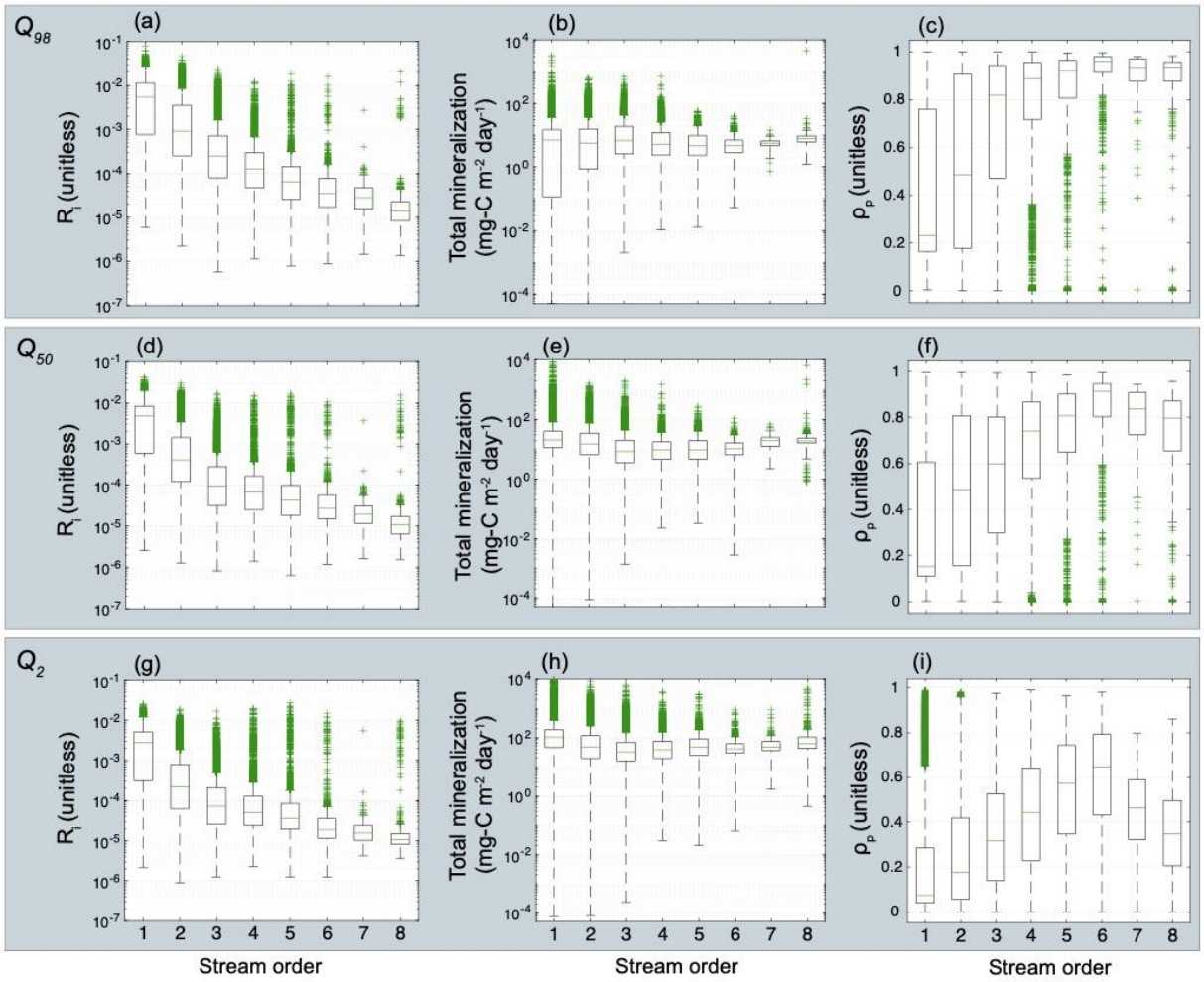

Figure 3: Relative elimination (R_i) (panels a, d and g), total mineralization (panels b, e, and h), and the proportion of total mineralization from photomineralization (ρ_p) for Q_{98} flows (panels a-c), Q_{50} flows (panels d-f), and Q_2 flows (g-i), for riverine reaches in the Connecticut River watershed.

3.4 Whole watershed DOC uptake

Using CUPS-OF-DOC, we can conceptualize DOC sources and uptake across the watershed (Fig. 4), building on the framework for drainage network ecological dynamics across stream orders and flows formalized in the River Continuum Concept (Vannote et al., 1980). Notably, the model summarizes the general lack of change in the absolute magnitude of total mineralization across

stream orders (Fig. 3b, e, h), with stream order-specific R_i changing in response to an increased DOC flux through each reach, perpetuated by a surplus of DOC added to the river network via terrestrial loading and GPP, relative to the amount of uptake (Table 2), rather than a change in DOC uptake reactivity. We note that our hydrologic and biogeochemical conceptualizations do not explicitly account for loss or addition of DOC via groundwater discharge or recharge in specific stream reaches. While our calibration of terrestrial loading implicitly accounts for terrestrial DOC sources via groundwater intrusion, it only reflects the extent of groundwater infiltration in the calibration reaches and applies these dynamics to the whole watershed (Section S2). In reaches with high groundwater recharge, R_i may be underestimated by our model, as we are not accounting for a groundwater DOC sink term, and vice versa in groundwater discharge reaches where we are not accounting for a DOC source term. Our conceptual model emphasizes the proportional increase in magnitude of the total mineralization flux at low and high stream orders as flows increase, while illustrating how the interplay between biomineralization and photomineralization drive ρ_p differently across flows and orders. Fig. 4 shows that terrestrial DOC loading (normalized by adjacent contributing area, $ter_{A,i}$) is nearly constant across stream orders, but again increases universally as flows increase. Thus, when considering total mineralization, $ter_{A,i}$, and GPP, only GPP changes significantly along the river network from low to high order, becoming important enough in high order streams at low flows to result in net autotrophy (P/R > 1) (Hosen et al., 2019).

The overall importance of photomineralization in terms of whole watershed DOC uptake increases in the winter when respiration fluxes are suppressed, with riverine and lake photomineralization maximized at Q_{98} flows in February, accounting for 69.9% and 9.6% of the total DOC uptake,

693 respectively (Table 2, Fig. 4). Average lake and river k_ψ values are highest in winter low flow
694 conditions (Table 2), with average riverine k_ψ exceeding lake k_ψ in all conditions, due mainly to
695 the absence of much canopy cover and shallow river depths. Despite the higher relative importance
696 of photomineralization in the winter at low flows, the overall magnitudes of DOC being taken up
697 during these conditions is the lowest compared with summer months and higher flows (Table 2),
698 because of lower DOC availability from low terrestrial and GPP sources fluxes (Table 2).
699 Regardless of flow, however, in February photomineralization in rivers always accounts for at
700 least half of the whole-watershed DOC uptake. Overwhelmingly, summer DOC uptake is
701 dominated by lake biomineralization, accounting for 80±1% of total uptake across all flows. River
702 biomineralization and lake photomineralization represent the lowest pathways of whole watershed
703 DOC uptake across flows and seasons, with lake photomineralization never exceeding 10% of the
704 total uptake, and river biomineralization maximized at 11.5% of uptake in summer at Q_2 flows,
705 due to warm water temperatures and ample fresh DOC (Table 2). Interestingly, average k_r values
706 in rivers exceed those in lakes in all conditions (Table 2), indicating that the residence time control
707 on biomineralization outweighs the DOC lability control, which in turn results in higher absolute
708 and relative DOC biomineralization fluxes in lakes than rivers in all conditions.

Our results show that lakes do not clearly fit into the River Continuum Concept framework for DOC biogeochemistry, but rather could be considered as "nodes" of variable reactivity dependent on the water residence time rather than stream order (a proxy for size) and flow. While large lakes do tend to occur more often on high stream orders, residence times can vary substantially across stream orders as they depend on both flow and lake volume, and the anthropogenic nature of reservoirs further complicate any potential lake-stream order relationships that may exist. Given the disproportionately large magnitude of summer GPP and respiration fluxes in lakes compared with rivers, whole-watershed frameworks for river network biogeochemical and ecological dynamics cannot neglect to consider the interconnectedness of lakes and rivers along the aquatic continuum. For example, of the whole-watershed DOC uptake taking place in August at Q_{50} flows, 82.7% takes place in lakes (Table 2), despite accounting for 5.5% of the total open water surface area within the watershed (Table S2).

Table 2: Summary of model outputs for the whole Connecticut River watershed, including total source and sink fluxes by each mechanism for all rivers and all lakes, percentage of the uptake via each mechanism, average per-reach elimination (R_i) for the whole watershed in lakes or rivers, and average watershed k_ψ and k_r for rivers and lakes. Results are given for median and extreme flow scenarios in August and February.

Description of flux or parameter	***Q*98**		***Q*50**		***Q*2**	
	February	**August**	**February**	**August**	**February**	**August**
Lake GPP flux (mg-C day^{-1})	3.5 x 10^{9}	1.8 x 10^{11}	7.8 x 10^{9}	3.4 x 10^{11}	3.7 x 10^{10}	1.5 x 10^{12}
River GPP flux (mg-C day^{-1})	1.2 x 10^{9}	2.1 x 10^{10}	2.4 x 10^{9}	2.6 x 10^{10}	8.3 x 10^{9}	6.6 x 10^{10}
Lake terrestrial load (mg-C day^{-1})	5.9 x 10^{9}	6.6 x 10^{9}	3.1 x 10^{10}	5.3 x 10^{10}	3.8 x 10^{11}	6.4 x 10^{11}
River terrestrial load (mg-C day^{-1})	6.9 x 10^{10}	8.4 x 10^{10}	3.0 x 10^{11}	5.4 x 10^{11}	3.5 x 10^{12}	6.4 x 10^{12}
Total watershed DOC source flux (mg-C day^{-1})	8.0 x 10^{10}	2.9 x 10^{11}	3.4 x 10^{11}	9.6 x 10^{11}	3.9 x 10^{12}	8.6 x 10^{12}
Lake photomin (mg-C day^{-1})	2.9 x 10^{7}	1.4 x 10^{8}	9.9 x 10^{7}	4.0 x 10^{8}	6.9 x 10^{8}	2.3 x 10^{9}
River photomin (mg-C day^{-1})	2.1 x 10^{8}	3.5 x 10^{8}	7.4 x10^{8}	1.2 x 10^{9}	4.1 x 10^{9}	5.7 x 10^{9}
Lake biomin (mg-C day^{-1})	5.7 x 10^{7}	2.4 x 10^{9}	2.5 x 10^{8}	8.6 x 10^{9}	2.9 x 10^{9}	8.4 x 10^{10}
River biomin (mg-C day^{-1})	4.6 x 10^{6}	8.4 x 10^{7}	3.0 x 10^{7}	6.9 x 10^{8}	5.2 x 10^{8}	1.2 x 10^{10}
Total watershed DOC uptake (mg-C day^{-1})	3.0 x 10^{8}	3.0 x 10^{9}	1.1 x 10^{9}	1.1 x 10^{10}	8.2 x 10^{9}	1.0 x 10^{11}
% of total watershed uptake via lake photomin	9.6%	4.7%	8.9%	3.7%	8.4%	2.2%
% of total watershed uptake via river photomin	69.9%	11.8%	66.1%	11.0%	50.0%	5.5%
% of total watershed uptake via lake biomin	19.0%	80.7%	22.3%	79.0%	35.3%	80.8%
% of total watershed uptake via river biomin	1.5%	2.8%	2.7%	6.3%	6.3%	11.5%
Average lake elimination (R_i, unitless)	0.0056	0.047	0.0045	0.039	0.003	0.022
Average per-reach river elimination (R_i, unitless)	8.6 x 10^{-4}	0.0035	5.9 x 10^{-4}	0.003	3.1 x 10^{-4}	0.002
Average lake k_ψ (day^{-1})	0.051	0.022	0.024	0.010	0.013	0.0058
Average river k_ψ (day^{-1})	0.087	0.037	0.076	0.033	0.067	0.029
Average lake k_r (day^{-1})	5.9 x 10^{-4}	0.0051	0.0014	0.013	0.0028	0.029
Average river k_r (day^{-1})	0.0021	0.022	0.0044	0.046	0.0080	0.084

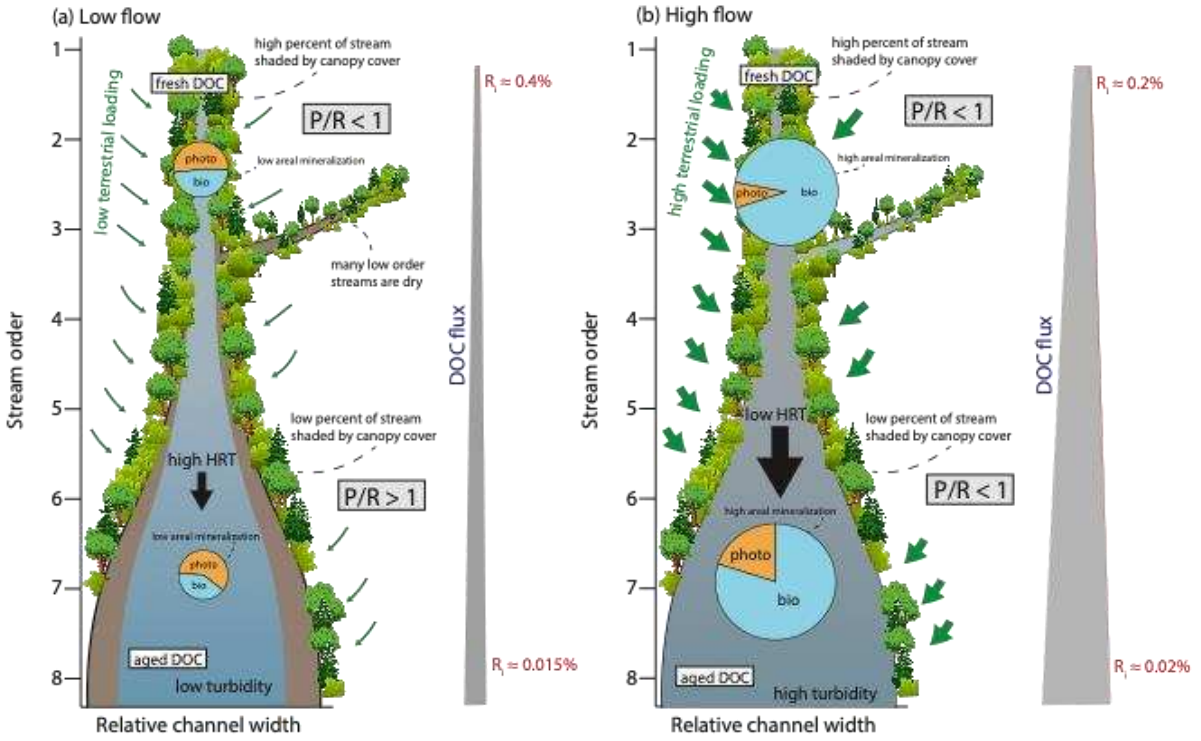

Figure 4: Conceptual model of growing seasonal riverine DOC dynamics at low and high flows according to stream order, as in the River Continuum Concept.

4. Implications and Conclusions

The CUPS-OF-DOC model enables a more unified theory of river network controls on DOC biogeochemical cycling across spatial and temporal scales. Because river/lake network morphometry constitutes the backbone of our model, it therefore exerts a fundamental control on the eventual sources, sinks and fluxes of DOC. In this study, we have focused specifically on presenting drivers of DOC uptake in rivers and lakes, as contextualized by the flux of total DOC moving through a watershed, and the relative importance of uptake mechanisms for ecosystem metabolism. We have shown that the relative elimination of DOC via mineralization, R_i, in rivers decreases with stream order, despite the near-constant total mineralization flux through stream orders.

735 We show that lake biomineralization dominates DOC uptake across flows in the summer,
736 accounting for 80% of all watershed uptake in August, despite representing <6% of the watershed
737 open water surface area. This finding strongly implies that research focusing on watershed carbon
738 dynamics can no longer treat lakes and rivers as separate components, as has been frequently the
739 norm. Large-scale watershed models that predict carbon dioxide or methane emissions from
740 headwaters to the outlet but skip over the impacts of lakes in their downstream flux calculations,
741 are missing the majority of DOC uptake in watersheds. The consequence of this oversight could
742 either be underestimating the magnitude of DOC sources to fit observed data, or overestimating
743 greenhouse gas emissions because calculated fluxes are too high.
744
745 We also show that in cold weather and especially at low flows, photomineralization in both rivers
746 and lakes becomes more important in terms of whole watershed DOC uptake, accounting for close
747 to 79.5% of all watershed DOC uptake in February at Q_{98} flows, and at least 50% in February
748 across all flows. Photomineralization is maximized when shallow river depths and low DOC
749 concentrations allow most or all of the water column DOC to be exposed to sunlight, and in winter
750 months when canopy cover is low. Studies focused on temperate watershed DOC uptake,
751 particularly in rivers, cannot neglect or assume negligible photomineralization compared with
752 respiration. Our results also indicate that flow can dramatically alter the proportion of total
753 mineralization that is from photomineralization, suggesting that temporally limited data cannot be
754 used to draw year-round conclusions regarding the relative importance of each mineralization
755 mechanism or overall ecosystem metabolism.
756

Our model output shows that photomineralization is the dominant uptake mechanism in the river reaches of this temperate, forested watershed, with relative photomineralization (ρ_p) maximized at low flows in 6th-order rivers. Our results suggests that river mineralization studies which focus exclusively on respiration are probably failing to account for a large portion, if not a majority, of the total riverine mineralization taking place. Based on our findings showing that photomineralization is especially important in winter in small streams at low flow, we hypothesize that photomineralization represents an even more dominant contributor to total mineralization in boreal and Arctic streams. Using a network-scale model like CUPS-OF-DOC, we have shown that robustly incorporating seasonality and flow differences into analyses of DOC uptake can help potentially reconcile existing, seemingly contradictory field studies, providing a larger context for the contributing drivers of photomineralization vs. biomineralization.

References

Abril, G. and Borges, A.V. (2019) Ideas and perspectives: Carbon leaks from flooded land: do we need to replumb the inland water active pipe? Biogeosciences 16, 769-784.

Aho, K., Fair, J., Hosen, J., Kyzivat, E., Logozzo, L., Weber, L., Yoon, B. and Raymond, P. (2021a) Distinct concentration-discharge dynamics in temperate streams and rivers: CO2 exhibits chemostasis while CH4 exhibits source limitation due to temperature control. Limnology and Oceanography 66, 3656-3668.

Aho, K.S., Hosen, J.D., Logozzo, L.A., McGillis, W.R. and Raymond, P.A. (2021b) Highest rates of gross primary productivity maintained despite CO2 depletion in a temperate river network. Limnology and Oceanography Letters 6, 200-206.

Allesson, L., Koehler, B., Thrane, J.E., Andersen, T. and Hessen, D.O. (2020) The role of photomineralization for CO2 emissions in boreal lakes along a gradient of dissolved organic matter. Limnology and Oceanography.

Appling, A.P., Hall Jr, R.O., Yackulic, C.B. and Arroita, M. (2018) Overcoming equifinality: Leveraging long time series for stream metabolism estimation. Journal of Geophysical Research: Biogeosciences 123, 624-645.

Baines, S.B. and Pace, M.L. (1991) The production of dissolved organic matter by phytoplankton and its importance to bacteria: patterns across marine and freshwater systems. Limnology and Oceanography 36, 1078-1090.

Battin, T.J., Luyssaert, S., Kaplan, L.A., Aufdenkampe, A.K., Richter, A. and Tranvik, L.J. (2009) The boundless carbon cycle. Nature Geoscience 2, 598.

Behrenfeld, M.J. and Falkowski, P.G. (1997) A consumer's guide to phytoplankton primary productivity models. Limnology and Oceanography 42, 1479-1491.

Beighley, R.E., Eggert, K.G., Dunne, T., He, Y., Gummadi, V. and Verdin, K.L. (2009) Simulating hydrologic and hydraulic processes throughout the Amazon River Basin. Hydrological Processes 23, 1221-1235.

Berggren, M., Lapierre, J.-F. and del Giorgio, P.A. (2012) Magnitude and regulation of bacterioplankton respiratory quotient across freshwater environmental gradients. The ISME Journal 6, 984-993.

Bertuzzo, E., Helton, A.M., Hall Jr, R.O. and Battin, T.J. (2017) Scaling of dissolved organic carbon removal in river networks. Advances in water resources 110, 136-146.

Brinkerhoff, C., Gleason, C. and Ostendorf, D. (2019) Reconciling at-a-station and at-many-stations hydraulic geometry through river-wide geomorphology. Geophysical Research Letters 46, 9637-9647.

Brinkerhoff, C., Raymond, P., Maavara, T., Ishitsuka, Y., Aho, K. and Gleason, C. (2021) Lake Morphometry and River Network Controls on Evasion of Terrestrially Sourced Headwater CO2. Geophysical Research Letters 48, e2020GL090068.

Buto, S.G. and Anderson, R.D. (2020) NHDPlus High Resolution (NHDPlus HR)---A hydrography framework for the Nation. US Geological Survey.

Casas-Ruiz, J.P., Catalán, N., Gómez-Gener, L., von Schiller, D., Obrador, B., Kothawala, D.N., López, P., Sabater, S. and Marcé, R. (2017) A tale of pipes and reactors: Controls on the in-stream dynamics of dissolved organic matter in rivers. Limnology and Oceanography 62, S85-S94.

Catalán, N., Marcé, R., Kothawala, D.N. and Tranvik, L.J. (2016) Organic carbon decomposition rates controlled by water retention time across inland waters. Nature Geoscience 9, 501.

Clay, C., Deininger, M., Hafner, J. and Nedeau, E. (2006) The Connecticut River watershed: Conserving the heart of New England: The Trust for Public Land.

Cole, J.J., Prairie, Y.T., Caraco, N.F., McDowell, W.H., Tranvik, L.J., Striegl, R.G., Duarte, C.M., Kortelainen, P., Downing, J.A. and Middelburg, J.J. (2007) Plumbing the global carbon cycle: integrating inland waters into the terrestrial carbon budget. Ecosystems 10, 172-185.

Coles, J.F. and Jones, R.C. (2000) Effect of temperature on photosynthesis-light response and growth of four phytoplankton species isolated from a tidal freshwater river. Journal of Phycology 36, 7-16.

819 Cory, R.M. and Kling, G.W. (2018) Interactions between sunlight and microorganisms influence
820 dissolved organic matter degradation along the aquatic continuum. Limnology and
821 Oceanography Letters 3, 102-116.
822 Cory, R.M., Ward, C.P., Crump, B.C. and Kling, G.W. (2014) Sunlight controls water column processing
823 of carbon in arctic fresh waters. Science 345, 925-928.
824 Creed, I.F., McKnight, D.M., Pellerin, B.A., Green, M.B., Bergamaschi, B.A., Aiken, G.R., Burns, D.A.,
825 Findlay, S.E., Shanley, J.B. and Striegl, R.G. (2015) The river as a chemostat: fresh perspectives
826 on dissolved organic matter flowing down the river continuum. Canadian Journal of Fisheries
827 and Aquatic Sciences 72, 1272-1285.
828 Demars, B.O. (2019) Hydrological pulses and burning of dissolved organic carbon by stream respiration.
829 Limnology and Oceanography 64, 406-421.
830 Dingman, S.L. (2007) Analytical derivation of at-a-station hydraulic–geometry relations. Journal of
831 Hydrology 334, 17-27.
832 Fasching, C., Ulseth, A.J., Schelker, J., Steniczka, G. and Battin, T.J. (2016) Hydrology controls
833 dissolved organic matter export and composition in an Alpine stream and its hyporheic zone.
834 Limnology and oceanography 61, 558-571.
835 Futter, M., Starr, M., Forsius, M. and Holmberg, M. (2008) Modelling the effects of climate on long-term
836 patterns of dissolved organic carbon concentrations in the surface waters of a boreal catchment.
837 Hydrology and Earth System Sciences 12, 437-447.
838 Gardner, J., Pavelsky, T. and Doyle, M. (2019) The abundance, size, and spacing of lakes and reservoirs
839 connected to river networks. Geophysical Research Letters 46, 2592-2601.
840 Gleason, C.J. (2015) Hydraulic geometry of natural rivers: A review and future directions. Progress in
841 Physical Geography 39, 337-360.
842 Gueymard, C. (1995) SMARTS2: a simple model of the atmospheric radiative transfer of sunshine:
843 algorithms and performance assessment. Florida Solar Energy Center Cocoa, FL.
844 Gueymard, C.A. (2019) The SMARTS spectral irradiance model after 25 years: New developments and
845 validation of reference spectra. Solar Energy 187, 233-253.
846 Hanson, P.C., Hamilton, D.P., Stanley, E.H., Preston, N., Langman, O.C. and Kara, E.L. (2011) Fate of
847 allochthonous dissolved organic carbon in lakes: a quantitative approach. PLoS One 6, e21884.
848 Harrison, J.A., Caraco, N. and Seitzinger, S.P. (2005) Global patterns and sources of dissolved organic
849 matter export to the coastal zone: Results from a spatially explicit, global model. Global
850 Biogeochemical Cycles 19.
851 Hirsch, R.M., Moyer, D.L. and Archfield, S.A. (2010) Weighted regressions on time, discharge, and
852 season (WRTDS), with an application to Chesapeake Bay river inputs. JAWRA Journal of the
853 American Water Resources Association 46, 857-880.
854 Hosen, J., Aho, K., Appling, A., Creech, E., Fair, J., Hall Jr, R., Kyzivat, E., Lowenthal, R., Matt, S. and
855 Morrison, J. (2019) Enhancement of primary production during drought in a temperate
856 watershed is greater in larger rivers than headwater streams. Limnology and Oceanography 64,
857 1458-1472.
858 Hosen, J., Aho, K., Fair, J., Kyzivat, E., Matt, S., Morrison, J., Stubbins, A., Weber, L., Yoon, B. and
859 Raymond, P. (2021) Source Switching Maintains Dissolved Organic Matter Chemostasis Across
860 Discharge Levels in a Large Temperate River Network. Ecosystems.
861 Howarth, R. and Michaels, A. (2000) The measurement of primary production in aquatic ecosystems, in:
862 Sala, O., Jackson, R., Mooney, H., Howarth, R. (Eds.), Meathods in Ecosystem Science.
863 Springer Science & Business Media, New York, p. 74.
864 Kaplan, L. and Cory, R. (2016) Dissolved organic matter in stream ecosystems: forms, functions, and
865 fluxes of watershed Tea, Stream ecosystems in a changing environment. Elsevier, pp. 241-320.
866 Koehler, B., Landelius, T., Weyhenmeyer, G.A., Machida, N. and Tranvik, L.J. (2014) Sunlight-induced
867 carbon dioxide emissions from inland waters. Global Biogeochemical Cycles 28, 696-711.

Koehler, B., von Wachenfeldt, E., Kothawala, D. and Tranvik, L.J. (2012) Reactivity continuum of dissolved organic carbon decomposition in lake water. Journal of Geophysical Research: Biogeosciences 117.

Leopold, L.B. and Maddock, T. (1953) The hydraulic geometry of stream channels and some physiographic implications. US Government Printing Office.

Lewis Jr, W.M. (2011) Global primary production of lakes: 19th Baldi Memorial Lecture. Inland Waters 1, 1-28.

Lin, P., Pan, M., Beck, H.E., Yang, Y., Yamazaki, D., Frasson, R., David, C.H., Durand, M., Pavelsky, T.M. and Allen, G.H. (2019) Global reconstruction of naturalized river flows at 2.94 million reaches. Water resources research 55, 6499-6516.

Maavara, T., Lauerwald, R., Regnier, P. and Van Cappellen, P. (2017) Global perturbation of organic carbon cycling by river damming. Nature communications 8.

Maavara, T., Logozzo, L., Stubbins, A., Aho, K., Brinkerhoff, C., Hosen, J. and Raymond, P. (2021) Does photomineralization of dissolved organics matter in temperate rivers? Journal of Geophysical Research: Biogeosciences.

Marzadri, A., Dee, M.M., Tonina, D., Bellin, A. and Tank, J.L. (2017) Role of surface and subsurface processes in scaling N2O emissions along riverine networks. Proceedings of the National Academy of Sciences 114, 4330-4335.

Mineau, M.M., Wollheim, W.M., Buffam, I., Findlay, S.E., Hall Jr, R.O., Hotchkiss, E.R., Koenig, L.E., McDowell, W.H. and Parr, T.B. (2016) Dissolved organic carbon uptake in streams: A review and assessment of reach-scale measurements. Journal of Geophysical Research: Biogeosciences 121, 2019-2029.

Moody, J.A. and Troutman, B.M. (2002) Characterization of the spatial variability of channel morphology. Earth Surface Processes and Landforms: The Journal of the British Geomorphological Research Group 27, 1251-1266.

Moore, R.B., McKay, L.D., Rea, A.H., Bondelid, T.R., Price, C.V., Dewald, T.G. and Johnston, C.M. (2019) User's guide for the national hydrography dataset plus (NHDPlus) high resolution. US Geological Survey.

Raymond, P.A., Hartmann, J., Lauerwald, R., Sobek, S., McDonald, C., Hoover, M., Butman, D., Striegl, R., Mayorga, E. and Humborg, C. (2013) Global carbon dioxide emissions from inland waters. Nature 503, 355.

Raymond, P.A., Saiers, J.E. and Sobczak, W.V. (2016) Hydrological and biogeochemical controls on watershed dissolved organic matter transport: Pulse-shunt concept. Ecology 97, 5-16.

Raymond, P.A. and Spencer, R.G. (2015) Riverine DOM, Biogeochemistry of marine dissolved organic matter. Elsevier, pp. 509-533.

Regnier, P., Friedlingstein, P., Ciais, P., Mackenzie, F.T., Gruber, N., Janssens, I.A., Laruelle, G.G., Lauerwald, R., Luyssaert, S. and Andersson, A.J. (2013) Anthropogenic perturbation of the carbon fluxes from land to ocean. Nature geoscience 6, 597.

Reynolds, C.S. (2006) The ecology of phytoplankton. Cambridge University Press.

Rocher-Ros, G., Harms, T.K., Sponseller, R.A., Väisänen, M., Mörth, C.M. and Giesler, R. (2020) Metabolism overrides photo-oxidation in CO2 dynamics of Arctic permafrost streams. Limnology and Oceanography.

Schlesinger, W.H. and Melack, J.M. (1981) Transport of organic carbon in the world's rivers. Tellus 33, 172-187.

Searcy, J.K. (1959) Flow-duration curves. US Government Printing Office.

Segatto, P.L., Battin, T.J. and Bertuzzo, E. (2021) The Metabolic Regimes at the Scale of an Entire Stream Network Unveiled Through Sensor Data and Machine Learning. Ecosystems, 1-18.

Sobek, S., Tranvik, L.J., Prairie, Y.T., Kortelainen, P. and Cole, J.J. (2007) Patterns and regulation of dissolved organic carbon: An analysis of 7,500 widely distributed lakes. Limnology and Oceanography 52, 1208-1219.

Stream Solute Workshop (1990) Concepts and methods for assessing solute dynamics in stream ecosystems. Journal of the North American Benthological Society 9, 95-119.
Tank, J.L., Rosi-Marshall, E.J., Griffiths, N.A., Entrekin, S.A. and Stephen, M.L. (2010) A review of allochthonous organic matter dynamics and metabolism in streams. Journal of the North American Benthological Society 29, 118-146.
USGS (2020) National Water Information System.
Vannote, R.L., Minshall, G.W., Cummins, K.W., Sedell, J.R. and Cushing, C.E. (1980) The river continuum concept. Canadian journal of fisheries and aquatic sciences 37, 130-137.
Vollenweider, R.A. (1970) Models for calculating integral photosynthesis and some inplications regarding structural properties of the community metabolism of aquatic systems. Prediction and measurement of photosynthetic prod.
Vollenweider, R.A. (1975) Input-output models. Schweizerische Zeitschrift für Hydrologie 37, 53-84.
Williams, P.l.B. and del Giorgio, P.A. (2005) Respiration in aquatic ecosystems: history and background. Respiration in aquatic ecosystems, 1-17.
Wollheim, W.M., Bernal, S., Burns, D.A., Czuba, J., Driscoll, C.T., Hansen, A., Hensley, R., Hosen, J., Inamdar, S. and Kaushal, S. (2018) River network saturation concept: factors influencing the balance of biogeochemical supply and demand of river networks. Biogeochemistry 141, 503-521.
Wollheim, W.M., Stewart, R.J., Aiken, G.R., Butler, K.D., Morse, N.B. and Salisbury, J. (2015) Removal of terrestrial DOC in aquatic ecosystems of a temperate river network. Geophysical Research Letters 42, 6671-6679.
Yoon, B., Hosen, J.D., Kyzivat, E.D., Fair, J.H., Weber, L.C., Aho, K.S., Lowenthal, R., Matt, S., Sobczak, W.V. and Shanley, J.B. (2021) Export of photolabile and photoprimable dissolved organic carbon from the Connecticut River. Aquatic Sciences 83, 1-17.
Zarnetske, J.P., Bouda, M., Abbott, B.W., Saiers, J. and Raymond, P.A. (2018) Generality of hydrologic transport limitation of watershed organic carbon flux across ecoregions of the United States. Geophysical Research Letters 45, 11,702-711,711.

946 **Acknowledgements**

947 This research was funded by the National Science Foundation (NSF) award no. 1340749, and a G.
948 Evelyn Hutchinson Fellowship to TM from the Yale Institute for Biospheric Studies (YIBS). The
949 Connecticut River watershed in located in Western Nehântick, Podunk, Siacog, Wappinger,
950 Massaco, Hammonasett, Pequot, Poquonock, Mohegan, Wangunk, Tunxis, Potomuc, Nipmuc,
951 Pennacook, Wabanaki, and Abenaki lands.

952

953 **Data availability:** The hydrological model and results are available at
954 https://zenodo.org/record/4135953#.YFqESOYpB24. The NHDPlus HR river network data is
955 available at https://www.usgs.gov/core-science-systems/ngp/national-hydrography/access-
956 national-hydrography-products. Connecticut River sampling site information, DOC concentration
957 and discharge data are available in the publication https://doi.org/10.1007/s10021-020-00514-7.
958 All measured discharge data and USGS-measured DOC concentrations are available on the USGS
959 NWIS data portal, https://waterdata.usgs.gov/nwis, using the USGS site IDs provided in Table 1.
960 All modeled DOC fluxes and model MATLAB code presented in this paper are in Dryad at
961 https://datadryad.org/stash/share/AJwJf1yc-Ds1We9nNjxngocEu9av797ceTUW0MfUgrY.

962

963 **Author contributions:** TM and PR conceptualized the research, JH, KA, LL, and PR collected
964 field data, TM and CB developed the model with input from all authors, and all authors contributed
965 to writing the paper.